

# AN INTERACTIVE SYSTEM FOR KINEMATIC ANALYSIS OF ARTIFICIAL JOINT IMPLANTS

<sup>1,2</sup>Mark Sarojak, M.S., <sup>1</sup>William Hoff, Ph.D., <sup>2</sup>Richard Komistek, Ph.D., and <sup>2</sup>Douglas Dennis, M.D.

<sup>1</sup>Colorado School of Mines, 1500 Illinois Ave, Golden, CO 80401.

<sup>2</sup>Rose Musculoskeletal Research Laboratory, 2425 South Colorado Blvd, Denver, CO 80220.

## Keywords

kinematic, arthroplasty, implant, optimization, software, polyethylene, simulated annealing.

## Abstract

The objective of this project was to develop and test a software system for the kinematic analysis of total joint arthroplasty (TJA) implants. Using a supervised iterative optimization algorithm (simulated annealing), the system iteratively adjusts the pose of an implant model to maximize correlation between the model's pose and the pose of an actual implant in a x-ray image. A graphical user interface (GUI) was developed that provides visualization of the model-fitting process, and permits human guidance for error correction. The resulting system was evaluated to determine its accuracy and repeatability. On synthetic images, the mean translational and rotational errors were found to be 0.005 mm and 0.0015 degrees, respectively. On *in vitro* images, the repeatability was found to be 0.15 mm of translation and 0.17 degrees of rotation. The outcome is a working joint-measurement software system and quantitative data to support comparison with other methods.

## 1 Introduction

Arthritis afflicts millions of people, often resulting in progressive joint destruction in which cartilage is worn away. This painfully debilitating condition is frequently treated with TJA, by replacing the arthritic joint with artificial implants (Figure 1).

Common to most implant designs is a polyethylene insert, which replaces the cartilage of the normal knee and provides a low friction rotational surface for the metallic implant components. It has been shown that many TJA failures are caused by excessive wear of this polyethylene insert. Specifically, the rapid wear of the polyethylene generates small particles,

which lead to osteolysis (bone decay) and loosening of the implant components [1][2].



Figure 1 Artificial knee implant, with tibial component (left) and femoral component (right). The white material is a polyethylene insert.

Although artificial knee joints are expected to last over 15 years, research indicates that many implants fail within 10 years [3]. It is believed that abnormal sliding and rotational motions of implanted knees may lead to excessively high shear stresses on the polyethylene, thus accelerating wear. Therefore, more knowledge of *in vivo* implant kinematics is needed so that implants that do not cause polyethylene failure can be designed.

Recently, x-ray fluoroscopy has been shown to be a useful tool for analyzing joint kinematics *in vivo* [2][4][5]. The fluoroscopic process creates a perspective projection, where metallic implants appear much darker than the soft tissues surrounding them (Figure 2), allowing direct observation of the implant components' silhouettes and their movements.



Figure 2 Fluoroscopy image of artificial knee.

There have been a number of algorithms described in the literature that estimate pose from silhouettes. Banks and Hodge [4] and Hoff *et al* [6] used two-dimensional template matching to measure the pose of knee implants in fluoroscopy images. Although successful, the template matching approach has a number of limitations. The precision of the orientation measurement is limited by the resolution of the library (typically around  $1^\circ$ ), and the accuracy may be further degraded by the use of a simplified perspective model. Also, the object's contour must be segmented from the image prior to matching. Finally, silhouette occlusions are not allowed, since a complete silhouette is needed to match the template.

Lavallee, *et. al.* [7] describes an algorithm which minimizes the 3-D distances between projection rays to the points on the contour, and the closest point on the surface of the object in its hypothesized pose (Figure 3). The algorithm is similar to the iterative closest point (ICP) approach of Besl and McKay [8], except that it uses 2-D image points as input instead of 3-D range data points. There are no limits on accuracy due to reliance on a template library, and this method can handle occlusion. However, the process is computationally intense, pre-segmentation of the object contour is still required, and a good initial estimate of the solution must be provided in order to converge to the correct solution (unable to escape local minima).

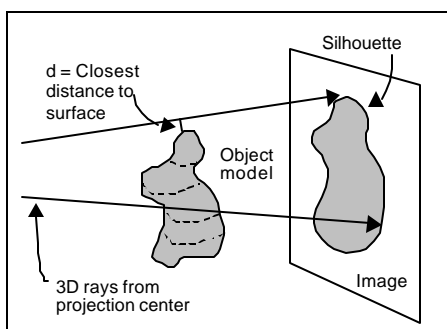


Figure 3 Distances are computed from the projection rays to the surface of the object, for the object's pose.

The purpose of this research was to develop and test a new fluoroscopy-based pose estimation method, which reduces or eliminates the problems of past techniques. Specifically, the new method was designed to improve upon the accuracy, speed, repeatability, and flexibility of previous methods.

## 2 Approach

Our overall approach is to use a supervised optimization algorithm to minimize the error between a predicted and an actual x-ray silhouette.

The choice of using a metric based on 2D measurements (rather than 3D) was motivated by the fact that modern computer graphics workstations (Silicon Graphics, Inc. Indigo2) can very quickly render 2D images of 3D objects ( $> 30$  Hz), even for highly complex models. By doing all computations in 2-D image space, we avoid expensive 3D computations of ray-to-surface distances.

We also wanted to avoid explicit pre-segmentation of the object silhouette in the image. In some cases, portions of the contour are difficult to extract automatically. This can be due to occlusions, or to the presence of adjacent material with similar contrast. For example, Figure 4 shows the magnitude of the gradient of the image in Figure 2. Note the incomplete silhouette of the tibial (lower) implant.

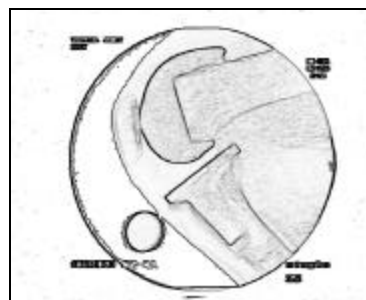


Figure 4 Gradient magnitude image.

Finally, we wished to completely remove the template library from the pose estimation process. First, template libraries require a lot of time to make and room to store (must have unique template for each and every implant model). Furthermore, they limit accuracy due to their limited resolutions and reliance upon interpolation. Finally, template-matching is incapable of handling images that contain partially occluded implant silhouettes (a common occurrence in fluoroscopy images... see Section 4).

Our approach incorporates the following elements: (1) a matching algorithm which numerically evaluates the match between the observed image and the predicted image from

the current hypothesized pose, (2) a robust optimization algorithm, and (3) a method of supervisory control. These elements are described in the following sections.

## 2.1 Matching Algorithm

To perform pose estimation, the matching algorithm requires two images as input. The first image is a predicted x-ray image, created using the implant CAD model. To render these images, the fluoroscope was modeled within the computer, using a software package named Open Inventor [9]. Figure 5 shows an example of a rendered image and its corresponding extracted silhouette.

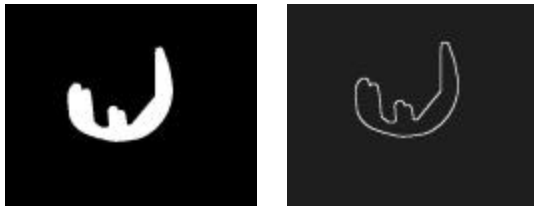


Figure 5 Predicted rendered image of the femoral model (left) and its silhouette (right).

The second input image is the actual x-ray image taken from the fluoroscope. Before matching, this image is inverted so that implant component pixels are white (as in the predicted image). Then an edge detection operation (Roberts) is also performed (Figure 6).

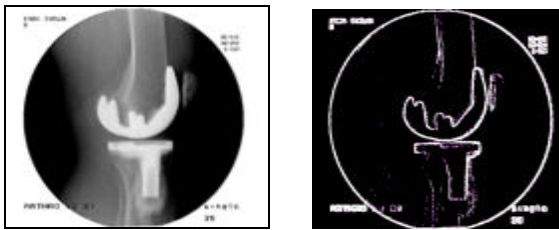


Figure 6 Input x-ray image, inverted (left) and edges (right).

To estimate the match between the input x-ray image and the predicted x-ray image, two image-processing operations are used. The first operation compares the pixel values of the two images, and the second operation evaluates the overlap of their contours (edges). Both scores are obtained by multiplying the two images together, summing the result, and normalizing by the sum of the predicted image. If  $G(x, y)$  is the input x-ray image (Figure 6, left) and  $H(x, y)$  is the predicted x-ray image (Figure 5, left), then the intensity matching score is:

$$\text{Intensity Matching Score} = \frac{\sum_{(x,y)} G(x, y)H(x, y)}{\sum_{(x,y)} H(x, y)}$$

The contour matching score is similarly calculated. If  $J(x, y)$  is the input contour image (Figure 6, right) and  $K(x, y)$  is the predicted contour image (Figure 5, right), then the edge matching score is:

$$\text{Contour Matching Score} = \frac{\sum_{(x,y)} J(x, y)K(x, y)}{\sum_{(x,y)} K(x, y)}$$

These two scores are then combined, with the contour matching value weighted more heavily than the area matching value. By weighting the contour score more heavily than the area value, the contour score dominates when the CAD models are close to the true solution. The weights of the intensity and contour scores were set to -1 and -2.67, respectively (determined experimentally)<sup>1</sup>.

The resulting total matching score then produces a distinct peak when the CAD model is exactly aligned with the image of the implant in the input x-ray image. Figure 7 is a 1D exhaustive plot of the matching score for an *in vitro* image (x-axis translation).

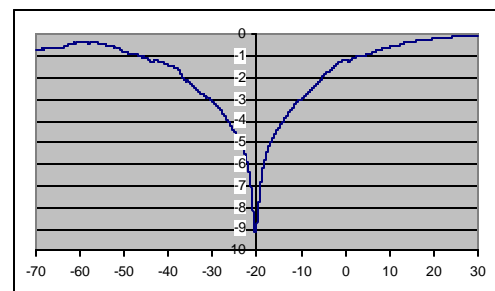


Figure 7 Matching score for an *in vitro* image as pose varies along x axis (dimensions in mm).

## 2.2 Optimization Algorithm

The choice of optimization algorithm depends on the characteristics of the function space to be

<sup>1</sup> Negative weights are used so that the best fit corresponds to a *minimum* of the objective function.

searched. Our function space is six dimensional (corresponding to the number of degrees of freedom in the model pose) and contains numerous local minima.

Figure 8 is an exhaustive plot of the matching score for an x-ray image, as the pose was varied in two rotational dimensions. Note the two large minima and many smaller local minima. The global minimum (the correct solution) is the deeper of the two large minima. The other large minimum is caused by the symmetry of the model (a tibial knee component), causing the silhouette to be very similar for two different orientations.

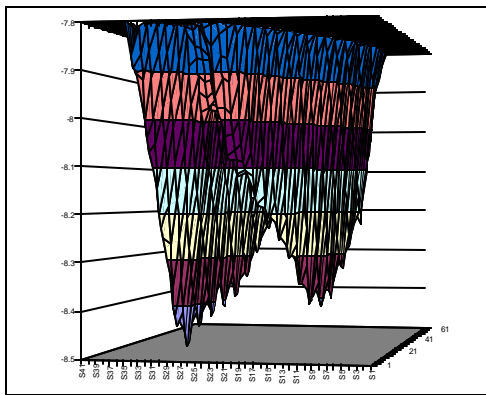


Figure 8 Matching scores for a x-ray image, as the x rotation and y-rotation angles were varied.

Figure 9 shows the x-ray image from which the matching scores were derived. The left image shows the tibial implant in the correct overlay position, which corresponds to the global minimum. The right image shows the tibial implant component in the incorrect position, which corresponds to the other large minimum (Figure 8). The two silhouettes are very similar, but different.

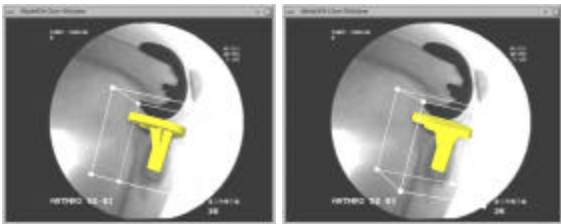


Figure 9 Overlays corresponding to the two large minima in the previous figure. (Left) Implant in correct pose. (Right) Incorrect pose.

To avoid these local minima, we selected a robust optimization algorithm called simulated

annealing [10]. This method is a modified version of the Nelder-Mead [11] (downhill simplex) optimization method. Simulated annealing employs a virtual temperature in order to escape local minima. Specifically, the virtual temperature is used to randomly make some solutions appear more favorable than they actually are. As the temperature iteratively decreases, this possibility of “uphill” movement decreases as well. In our application, the virtual temperature is decreased every ten iterations by multiplying the current temperature by 0.99. By slowly lowering the virtual temperature in this manner, the algorithm is allowed escape local minima while searching for the global minimum.

### 2.3 Supervisory Control

Although the optimization algorithm can escape most (shallow) local minima, it occasionally gets stuck in a deeper minimum. With a large enough temperature the algorithm could even escape these large minima; however, we have found it to be more efficient to use an interactive approach. In this approach, the human visually supervises the model-fitting process and can make corrections if necessary.

A graphical user interface was developed (Figure 10) that allows the user to visualize and control the model fitting process. Visualization is accomplished by displaying the model as an overlay on the x-ray image, and by continuously updating the model’s position with the current optimization solution.

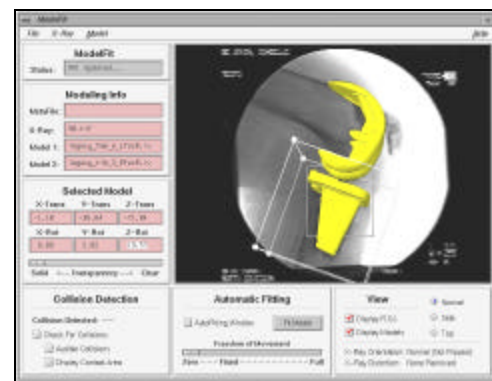


Figure 10 The graphical user interface allows the user to easily visualize and control the progress of the model fitting process.

If the system gets stuck in an incorrect pose, the user can temporarily seize control of the model

(using the mouse) and move it towards the correct pose. Releasing the mouse then allows the optimization algorithm to resume at the new pose. This initializes the state vector closer to the solution, saving time by reducing the number of iterations needed to be performed.

This approach is a form of *traded control* [12] which is used in supervised robot control. The philosophy is that the system incorporates the best of both approaches. It combines the speed and precision of the computer with the common sense and domain knowledge of the human. The resulting system is both efficient and reliable.

### 3 Results

Formal evaluations focused on determining the accuracy, reliability and speed of the system. In addition, the system was tested for systematic bias and dependence of the accuracy upon the pose of the CAD models.

A set of five synthetic x-ray images was created by rendering the CAD models in known poses. The images were corrupted with gaussian noise of magnitude equal to that observed in *in vivo* images (Figure 11).



Figure 11 Three of the synthetic images used in evaluations.

Five *in vitro* images were created using the fluoroscope. The implants were fixed in a constant (but unknown) relative position, and images were captured as the implants were moved through the fluoroscope (Figure 12).



Figure 12 Three of the *in vitro* images used in evaluations.

*In vivo* images were not used during formal evaluations because the relative pose of the implants within them is not constant (patient is moving) and can not be determined.

Three human subjects were used in the evaluations. Prior to beginning, participants were trained on use of the interactive system. Training included familiarization with a 6 degree of freedom spaceball (3D mouse), an explanation of the stopping criteria for each test, and a practice session using images similar to the test images. Each subject was allowed to practice until all subjects achieved the same ability level. During testing, the final pose (best fit) and elapsed time were recorded for each image. Table 1 summarizes the accuracy, repeatability and speed values obtained from experimentation.

Table 1 Summary of system performance (unlabeled units are in mm or degrees).

Accuracy (synthetic image)	Repeatability ( <i>in vitro</i> image)	Time per image (both types)
Translations: $\mu = 0.0053$ $\sigma = 0.0205$	Translations: $\sigma = 0.15$	Avg. user time: $\mu = 75$ sec $\sigma = 20.5$ sec
Rotations: $\mu = 0.0015$ $\sigma = 0.0117$	Rotations: $\sigma = 0.17$	Avg. total time: $\mu = 349.4$ sec $\sigma = 76.7$ sec

Statistical analysis showed no significant deviation of the data mean from zero, meaning that the system has no systematic bias ( $p=0.005$ ). However, the analysis showed that error was, in fact, dependent upon out-of-plane translation (error increases with negative z-axis translation). All other translations and rotations had no statistical effect on the error ( $p=0.005$ ).

### 4 Discussion

Several forms of occlusion are common in fluoroscopy images. The first form of occlusion results when implant silhouettes intersect each other due to the imaging perspective (see Figure 11, right). Another common form of occlusion is when an implant silhouette is partially off of the imaging plane (see Figure 13, left). This happens because the patients are in motion during fluoroscopic surveillance.

Our method is capable of handling images with partially occluded implant silhouettes. This is possible because the interactive system finds the maximum correlation between the silhouette of the synthetic x-ray image and the remaining portion of the occluded implant silhouette. Even though a portion of the silhouette is

occluded, the maximum correlation still occurs in the correct pose. Figure 13 illustrates this ability.

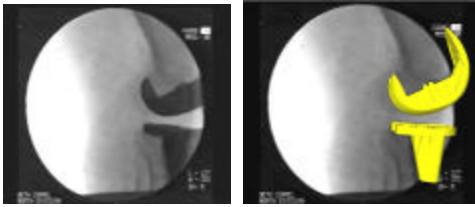


**Figure 13 Demonstration of successful overlay despite occlusion of implants.**

Additionally, an analysis on synthetic images containing 50% occlusion showed that the accuracy of the interactive system is the nearly the same for these images as for non-occluded images.

A suggestion for future research is to use a more efficient optimization algorithm. Simulated annealing, may visit incorrect solutions several times while performing function optimization. Other robust optimization algorithms exist, such as genetic algorithms [13], which may prove to be more efficient. Finally, we note that fluoroscopic image should be of good quality. Image distortion should be removed, and image clarity and contrast should be maximized in order to ensure accurate and reliable system performance.

The kinematic analysis system presented in this paper is currently being used at Rose Musculoskeletal Research Laboratory (Denver, CO) to study various types of joint implants, including hips, ankles and temporomandibular joints (Figure 14), as well as knees.

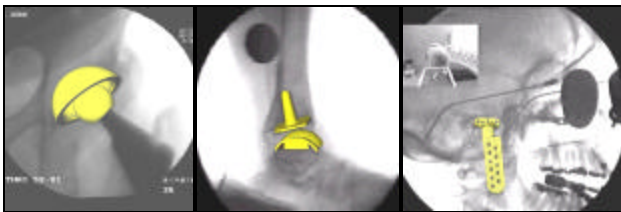


**Figure 14 Applications of the system to hips, ankles, and TMJ implants (left to right).**

## 5 References

- [1] Wright, T.M., C.M. Rinnac, and S.D. Stulberg, "Wear of Polyethylene in Total Joint Replacement. Observations from Retrieved PCA Knee Implants," *Clin Orthop*, Vol. 276, pp. 126-134, 1992.
- [2] Stiehl JB, Komistek RD, Dennis DA, Paxson RD, Hoff, WA, "Fluoroscopic analysis of kinematics after posterior-cruciate-retaining total knee arthroplasty using fluoroscopy," *J Bone Joint Surg*, 77B:884-889, 1995.
- [3] Landy MM, Walker PS., "Wear of ultra-high-molecular-weight polyethylene components of 90 retrieved knee prostheses," *J Arthroplasty* 3: suppl S73-85, 1988.
- [4] Banks, S.A., and W.A. Hodge, "Accurate Measurement of Three-Dimensional Knee Replacement Kinematics Using Single Plane Fluoroscopy," *IEEE Trans. Biomed. Eng.*, Vol. 43, no. 6, 1996.
- [5] Komistek, R.D., D.A. Dennis, S.A. Walker, and J.B. Stiehl, "A Determination of *In Vivo* Patellofemoral Contact Positions," *ORS Proceedings*, San Francisco, CA, 1997.
- [6] Hoff, W.A., R.D. Komistek, D.A. Dennis, S.M. Gabriel, and S.A. Walker, "*In Vivo* Pose Estimation of Artificial Knee Implants Using Computer Vision," *Clin Biomech*, Vol. 13, pp. 455-472, 1998.
- [7] Lavallee, S., R. Szeliski, and L. Brunie., "Anatomy-Based Registration of Three-Dimensional Medical Images, Range Images, X-ray Projections, and Three-Dimensional Models Using Octree-Splines," *Computer Integrated Surgery: Technology and Clinical Applications*, R. Taylor, Ed., Cambridge, Massachusetts, MIT Press, pp. 115-143, 1996.
- [8] Besl, P.J. and N.D. McKay, "A Method for Registration of 3D Shapes," *IEEE Trans. Patt. Anal. and Mach. Intell.*, 10(2):167-192, March 1985.
- [9] Wernecke, J., *The Inventor Mentor: Programming Object-Oriented 3D Graphics with Open Inventor*, 2nd Ed., Reading, Massachusetts, Addison Wesley, 1994.
- [10] Kirkpatrick, S., J. Gelatt, and M.P. Vecchi, "Optimization by Simulated Annealing," *Science*, Vol. 220, no. 4598, pp. 671-680, 1983.
- [11] Press, W.H., S.A. Teukolsky, W.T. Vetterling, and B.P. Flannery, *Numerical Recipes in C*, " 2 d Ed., Cambridge University Press, 1992.
- [12] Sheridan, T.B., *Telerobotics, automation, and human supervisory control*, Cambridge, Massachusetts, MIT Press, 1992.
- [13] Whitley, D., S. Rana, and R.B. Heckendorn, "Representation Issues in Neighborhood Search and Evolutionary Algorithms," *Strat. Eng. And Comp Sci*, pp. 39-57, 1998.